



ELSEVIER



Available online at [www.sciencedirect.com](http://www.sciencedirect.com)

ScienceDirect

Journal of the Franklin Institute 354 (2017) 8747–8757

[www.elsevier.com/locate/jfranklin](http://www.elsevier.com/locate/jfranklin)



# Ultra-broadband material spectroscopy from scattering parameters obtained from time domain measurements

Ajay Bandla<sup>a</sup>, Nathaniel Hager III<sup>b</sup>, Mohammad-Reza Tofighi<sup>a,\*</sup>

<sup>a</sup>*School of Science, Engineering, and Technology, Pennsylvania State University, Capital College, Middletown, PA 17057, USA*

<sup>b</sup>*Department of Physics and Engineering, Elizabethtown College, Elizabethtown, PA 17022, USA*

Received 31 July 2016; accepted 29 October 2016

Available online 3 November 2016

---

## Abstract

The relaxation phenomena (e.g. free and bond water relaxations) and the frequencies at which they occur (from kHz to GHz) can convey valuable information in dielectric spectroscopy for material process monitoring and biology research. Finding the ultra-broadband frequency domain reflection and transmission coefficients (scattering parameters) from time domain measurements can be challenging. The current approach, often employed by material scientists, involves numerical integration of Laplace transform of the time domain data. On the other hand, the more computationally efficient fast Fourier transform (FFT) techniques have been well-developed and widely used in the engineering community. In this study, we propose a novel method, based on FFT of non-uniformly sampled time domain reflectometry (TDR) data, to obtain the frequency domain information from kHz to GHz. We perform FFT operations on multiple time windows of fixed number of points. The time duration of each window is increased, and the sample rate is decreased progressively. We correct for the truncation errors using Nicolson ramp prior to applying the FFT. We combine the FFT's of these multiple windows to obtain a single spectrum for each sample. We test this method to known lossy materials and hydrating cement samples. The results are in close agreement with those obtained using direct numerical integration.

© 2016 The Franklin Institute. Published by Elsevier Ltd. All rights reserved.

---

\* Corresponding author.

## 1. Introduction

Dielectric spectroscopy at RF and microwave frequencies has many promising applications in biological or material research. Methods have been proposed to detect and differentiate certain biological cells [1–4]. For instance, microwave techniques have been successfully used to detect live and dead biological cells [1,2]. The biological samples are often probed using vector network analyzer (VNA) [2–4]. Valuable information on biological material properties including cell structure, dipolar relaxations, and membrane processes can be obtained by studying their frequency dependent complex dielectric permittivity. Dielectric spectroscopy has also been used for monitoring material curing process. For example, information about the chemical state of the material, and free and bond water can be determined by measuring the complex permittivity [5,6].

The measurement methodology for dielectric permittivity characterization can be conducted in two domains: time and frequency. Time domain methods involve transmission line reflection/transmission measurements. A known time domain reference signal (step or pulse) is incident on the transmission line, and the reflected or transmitted signal is measured using a fast sampler. In frequency domain measurement methods, a source launches a signal at a single frequency to the material under test. The receiver is used to detect the reflected or transmitted signal from the material, from which the magnitude and phase data at that frequency are produced. The source signal is then changed to the next frequency point and so on, resulting in a frequency sweep operation.

The frequency dependent dielectric permittivity of biological or lossy samples is often characterized using standard VNAs which can be expensive and may not cover low frequency kHz range. Time domain methods such as time domain reflectometry (TDR) are promising because of the relatively lower cost and feasibility of broadband material characterization, where ultra-wideband frequency data from kHz to a few tens of GHz can help in better identifying characteristics of biological cells or materials. For instance, a measurement system consisted of a pulse generator, sampling head, and a TDR oscilloscope [7] was used to study the evolution of the dielectric property of mammalian cell membranes after exposing the cells to pulsed electric fields. A similar measurement technique was used for complex permittivity measurement in hydrating cement for determining chemical state of water [5,6].

Monitoring the relaxation frequencies of materials can provide key information about their properties. There are various relaxation mechanisms, each of which is dominant over a certain frequency range. These relaxation mechanisms can extend over a broad range of frequencies. For example the relaxation frequencies for biological materials extend from kHz to GHz [8]. Maxwell–Wagner effect, and free and bond water dipolar rotation are relaxation phenomena in biological materials, which introduce a wide range of characteristic frequencies for various dispersions [8].

Different complex permittivity extraction methods from frequency domain data have been suggested in the literature [5,6,9]. In time domain TDR method, the time domain data from TDR measurements has to be transformed to the frequency domain to extract the dielectric property information. Current methods involve applying numerical integration of the Laplace (Fourier) transform [5–7,10,11]. These methods were successfully implemented to investigate the complex permittivity of various lossy samples from TDR measurements.

For the TDR method, time domain reflected signals data should be collected up to a few milliseconds to obtain kHz spectrum. On the other hand, for extending the spectral domain information to GHz range, very fine time resolution in the order of a few tens of picoseconds

is required during the rise time of the TDR pulse. This would result in an extremely large number of data points. To avoid this problem, multiple time scale sampling methods can be used [10], where the reflected signal is sampled in multiple segments each having a different sampling rate such that the sampling time progressively increases for longer elapsed times. Direct numerical integration of the Laplace (Fourier) transform is then used to transform the data to the frequency domain. As another approach, a numerical Fourier transform formula was used in [12] to handle the non-uniform sampling issue.

In this paper, we propose using an alternative and novel method based on the fast Fourier transform (FFT) to obtain the frequency domain information from the time domain TDR waveforms. The technique consists of time windows for FFT with progressively varying scale, where each window has a different sampling time. Section 2 describes our approach to obtain the broadband frequency domain information from the time domain measurements, where Nicolson ramp [13] is used for each window to correct for truncation errors. The measurement technique is described in Section 3. Measurements are done using an open-ended coaxial probe and a TDR (Fig. 1(a)), where multi-scale sampling time method is used to capture signals up to the millisecond time scale. This method is applied for two sample liquids, hydrating cement at two instances of its curing process, and the open probe serving as a reference [10]. These results are discussed in Section 4. Conclusion and discussion about the future work of this research are provided in Section 5. To the best of authors' knowledge, the utilization of the Nicolson ramp method to multi-window

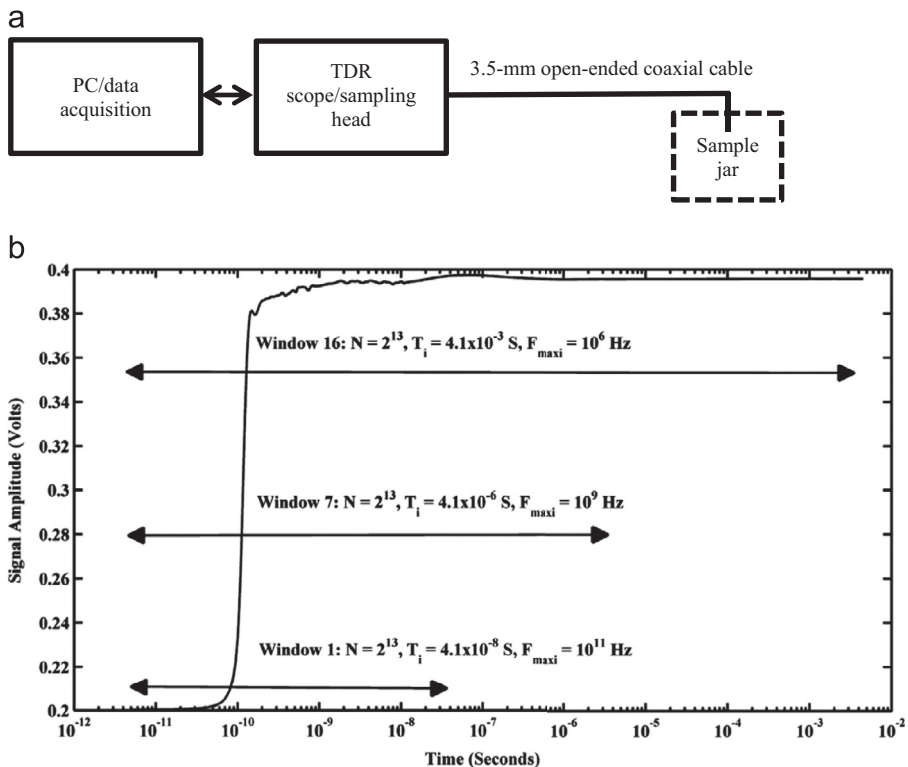


Fig. 1. a) Measurement setup. b) Parameters of the individual time windows for 1,2 dichloroethane. For a window 'i',  $T_i$  is the duration of the signal in seconds,  $N$  is the number of points for each window, and  $F_i$  is the maximum frequency range in the frequency domain (in Hz) that is provided by FFT.

FFT for obtaining ultra-broadband (over 6 orders of magnitude) spectral domain information from TDR data as described in this work has not been explored previously.

## 2. Approach

In order to transform the TDR data to the frequency domain, the non-uniformly sampled TDR measurement data should be acquired (Fig. 1a) from picosecond to millisecond range [10], as explained in the next section. Then, starting from zero time point, we choose a time window corresponding to the highest frequency from the frequency range of interest. We then resample this data on a uniform time scale and apply FFT to this data. We repeat these steps for multiple windows (Fig. 1b) of subsequently increasing time duration. The duration and sampling rate play a key factor in selecting the windows.

Our measurements involve a low permittivity and a high permittivity liquid mixture, namely 1,2 dichloroethane and a mixture of water and PMMA respectively [11]. The focus of this paper is on time to frequency domain transformation for material spectroscopy and obtaining the frequency domain reflection coefficient, from which the complex permittivity could be extracted. In this regard, the choice of these two liquids should be further clarified. It is well-known that reference liquids, which closely match the permittivity of the material under test (hydrating cement as an example in this paper) at the initial and end stages of cure, would provide more accurate extracted permittivity as discussed in [11]. In fresh cement paste, where water-loading and ion conductivity is high, a mixture of water and PMMA powder would be a good choice, while at longer cure times, the low permittivity 1,2-dichloroethane provides reduced permittivity comparable to the cured paste [11]. These two reference liquids set the high and low bounds for the spectral domain results for material spectroscopy over a wide range during the cure monitoring process. They cover a real permittivity range of approximately 10–100 from  $10^7$  to  $10^8$  Hz and 10–50 from  $10^8$  to  $10^{10}$  Hz, where free and bound water relaxations are occurring, which makes them suitable for permittivity extraction of cement samples as discussed in [11].

One main problem for taking FFT of the truncated TDR data is the spectral artifacts due to the step-like waveform for each window. To remedy this, the Nicolson ramp method [13] is used for each window on the step-like waveforms to correct for the truncation errors during the frequency domain transformation.

As mentioned before, the non-uniformly sampled measurement data (Section 3) is uniformly resampled (interpolated) over multiple windows. For each window  $i$ , we choose the time duration  $T_i$  and the sampling rate based on the requirement of maximum ( $F_{\max i}$ ) and minimum ( $F_{\min i}$ ), frequency content for each window provided by the FFT, where  $F_{\min i}$  ( $=1/T_i$ ) is the frequency resolution and  $F_{\max i} = NF_{\min i}/2$ .

Next, we apply the Nicolson ramp method [13] on each window of the uniformly resampled time domain data. A ramp signal  $r_i(t) = V_{di}r(t)$ , where  $r(t)$  is the unit ramp function, is considered for each window. Here,  $V_{di}$  is the voltage difference for the TDR signal level at time  $t = T_i$  with respect to the TDR signal level at time  $t=0$ . If the TDR voltage has a nonzero value at zero time, that would be also added to the ramp signal. The ramp signal (Fig. 2) is then subtracted from the TDR voltage signal  $v_i(t)$  (step response, Fig. 2) prior to applying the FFT to obtain a new signal  $\hat{v}_i(t)$  (deramped signal, Fig. 2):

$$\hat{v}_i(t) = v_i(t) - r_i(t) \quad (1)$$

Nicolson [13] infers that, since  $\sin k\pi = 0$  for integer  $k$ , at frequencies  $\omega = k\omega_0$  ( $\omega_0 = 2\pi/T_i = 2\pi F_{\min i}$ ), the Fourier transform of the deramped signal ( $\hat{V}_i(k\omega_0)$ ) is equal to the

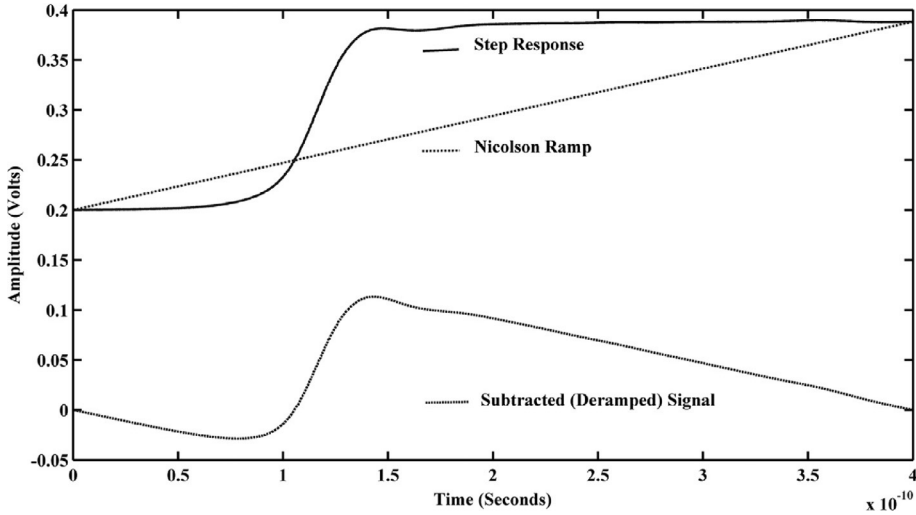


Fig. 2. Illustration of the Nicolson ramp method to remove artifacts due to truncation errors involved in fast Fourier transform of step-like waveforms.

Fourier transform of the TDR signal prior to subtracting the ramp ( $V_i(k\omega_{0i})$ ).

$$\begin{aligned}
 R_i(k\omega_{0i}) &= \left[ V_{di} \frac{2 \sin(\omega T_i/2)}{jT_i\omega^2} \exp\left(-\frac{j\omega T_i}{2}\right) \right]_{\omega=k\omega_{0i}} \\
 &= V_{di} \frac{2 \sin k\pi}{jT_i(k\omega_{0i})^2} \exp(-jk\pi) = 0
 \end{aligned}
 \tag{2}$$

$$\hat{V}_i(k\omega_{0i}) = V_i(k\omega_{0i}) - R_i(k\omega_{0i}) = V_i(k\omega_{0i})
 \tag{3}$$

The Fourier transform of  $\hat{V}_i(k\omega_{0i})$  ( $= V_i(k\omega_{0i})$ ) is obtained numerically using the well-known FFT algorithm [14], which would provide the Fourier transform for  $N$  frequency points ( $k=0, 1, \dots, N-1$ ), where  $N$  should be a power of 2 for computational efficiency [14]. Furthermore, subtracting the ramp signal from the step-like TDR voltage signal not only corrects for the truncation error but also eliminates the need for adding the Fourier transform of the ramp back to the Fourier transform of  $\hat{V}_i(k\omega_{0i})$  obtained by the FFT algorithm.

### 3. Measurement

An internal voltage step signal generated by the TDR is incident on the sample material. This signal travels through the cables, the open-ended coaxial probe [10] and onto the sample. The TDR sampling head measures the reflected signal. Measurements are performed using Agilent 54740 TDR oscilloscope with a 54754A differential plug-in. This has a 20 GHz detection bandwidth and a 35 ps internal voltage step. The sampling interval is set to start at a very low value, i.e. in picosecond range, since the initial reflected portion contains a high rise time signal. The sampling rate is increased in the subsequent segments as the voltage level approaches a constant value (Fig. 1b). A program gathers data from the TDR scope at various time scales. Each measurement record is taken on 12 different time segments, using 2000 points/segment (high resolution) at short elapsed times, and 200 points/segment (low

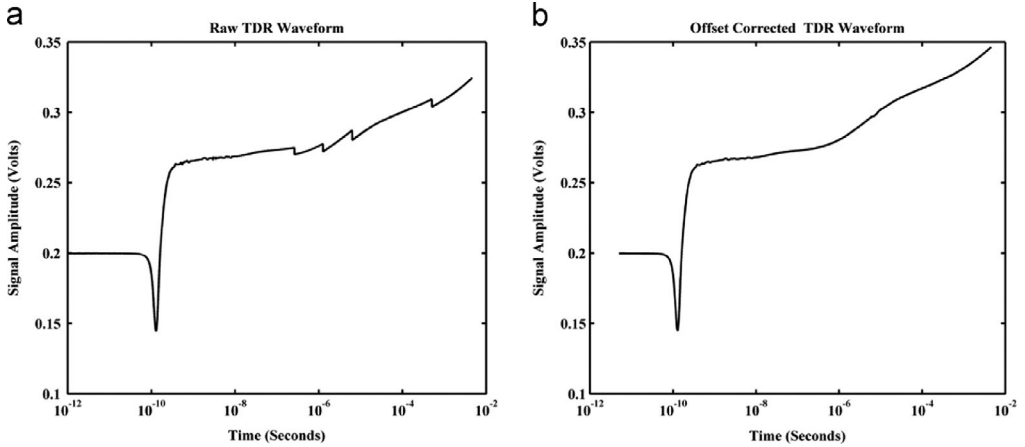


Fig. 3. a) TDR waveform data containing multiple segments of the water-PMMA sample. b) Offset corrected TDR waveform of the water-PMMA sample.

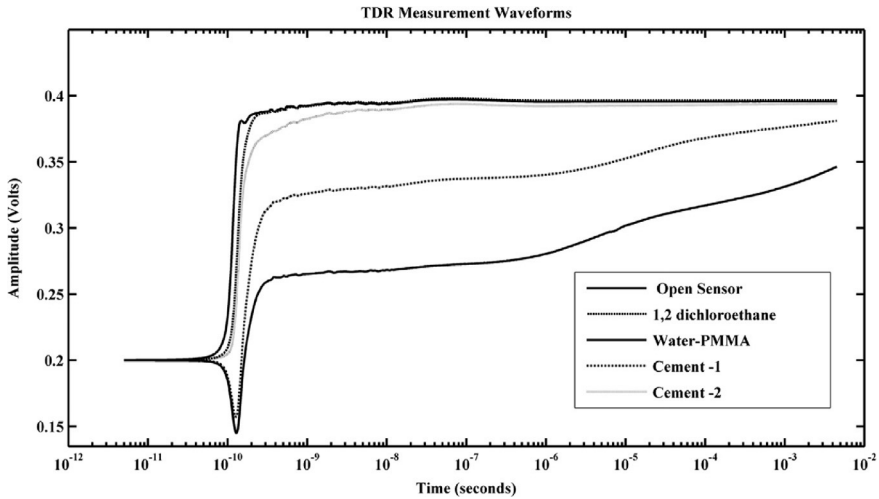


Fig. 4. TDR measurement waveforms of the test samples after offset correction.

resolution) at long elapsed times. The first segment is a timing reference of the incident pulse (high resolution), the second segment is the initial reflected signal (high resolution), and all remaining segments are continuations of the initial reflected signal at longer delay times (lower resolution). There are 11 segments in the reflected signal. The sampling interval for the second segment is 0.1 ps, and the third segment has 0.4 ps sampling interval. The sampling interval for the 9 subsequent segments are 2.5 ps, 10 ps, 20 ps, 250 ps, 1 ns, 5 ns, 25 ns, 2.5  $\mu$ s, and 25  $\mu$ s respectively. As previously mentioned, the measurements are taken for four samples, which are 1,2 dichloroethane, water-PMMA, cement paste 1, and cement paste 2, as well as the open (empty) probe. Cement pastes 1 and 2 are representative of two different times during cement curing process. We use the open measurement as the reference for relative reflection coefficient measurements [10] as explained later. The TDR voltage response has a

12-bit analog to digital conversion (ADC) resolution (4096 levels) corresponding to a voltage resolution in the order of 0.2 mV. Data collection and Laplace integration are performed using an executable program written in Visual C, while FFT's are performed using a program written in Matlab.

Vertical correction has to be performed to each segment to remove DC offsets which are introduced after combining measurements for individual segments. The raw measurement data is shown in Fig. 3(a). The time domain signal after performing the correction for the vertical offsets in the individual time segments is shown in Fig. 3(b). We also average the TDR signal information from repeated measurements prior to transforming to the frequency domain. A plot of TDR graphs of all the five samples after offset correction is shown in Fig. 4. A flowchart showing the operation is illustrated in Fig. 5.

The offset corrected data for each sample is then used to obtain the multiple windows as described in Section 2 (Fig. 1b), where after applying the Nicolson ramp correction to the time domain data for each of the time windows, we perform FFT on it. The  $F_{max\ i}$  values are chosen such that each decade of the frequency information is obtained from three FFT's. This would ensure a smoother transition from the FFT of a window to the FFT of the next window.

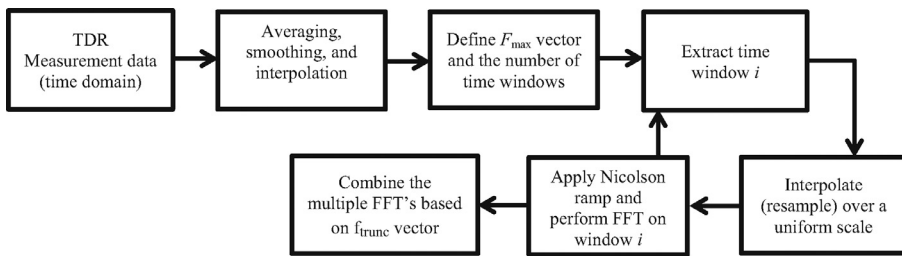


Fig. 5. Flowchart showing the sequence of operations to obtain broadband frequency domain data from TDR measurements.

Table 1

Parameters of each window showing  $F_{max\ i}$  and  $F_{trunc\ i}$  values.  $F_{max\ i}$  is the maximum frequency obtained by the FFT for the  $i$ th window, and  $F_{trunc\ i}$  is the truncation range for the  $i$ th window.

Window # $i$	$F_{max\ i}$ (Hz)	$F_{trunc\ i}$ (Hz)
1	$10^{11}$	$7 \times 10^8 - 25 \times 10^9$
2	$7 \times 10^{10}$	$5 \times 10^8 - 7 \times 10^8$
3	$4 \times 10^{10}$	$2 \times 10^8 - 5 \times 10^8$
4	$10^{10}$	$7 \times 10^7 - 2 \times 10^8$
5	$7 \times 10^9$	$5 \times 10^7 - 7 \times 10^7$
6	$4 \times 10^9$	$2 \times 10^7 - 5 \times 10^7$
7	$10^9$	$7 \times 10^6 - 2 \times 10^7$
8	$7 \times 10^8$	$5 \times 10^6 - 7 \times 10^6$
9	$4 \times 10^8$	$2 \times 10^6 - 5 \times 10^6$
10	$10^8$	$7 \times 10^5 - 2 \times 10^6$
11	$7 \times 10^7$	$5 \times 10^5 - 7 \times 10^5$
12	$4 \times 10^7$	$2 \times 10^5 - 5 \times 10^5$
13	$10^7$	$7 \times 10^4 - 2 \times 10^5$
14	$7 \times 10^6$	$5 \times 10^4 - 7 \times 10^4$
15	$4 \times 10^6$	$2 \times 10^4 - 5 \times 10^4$
16	$10^6$	$7 \times 10^3 - 2 \times 10^4$

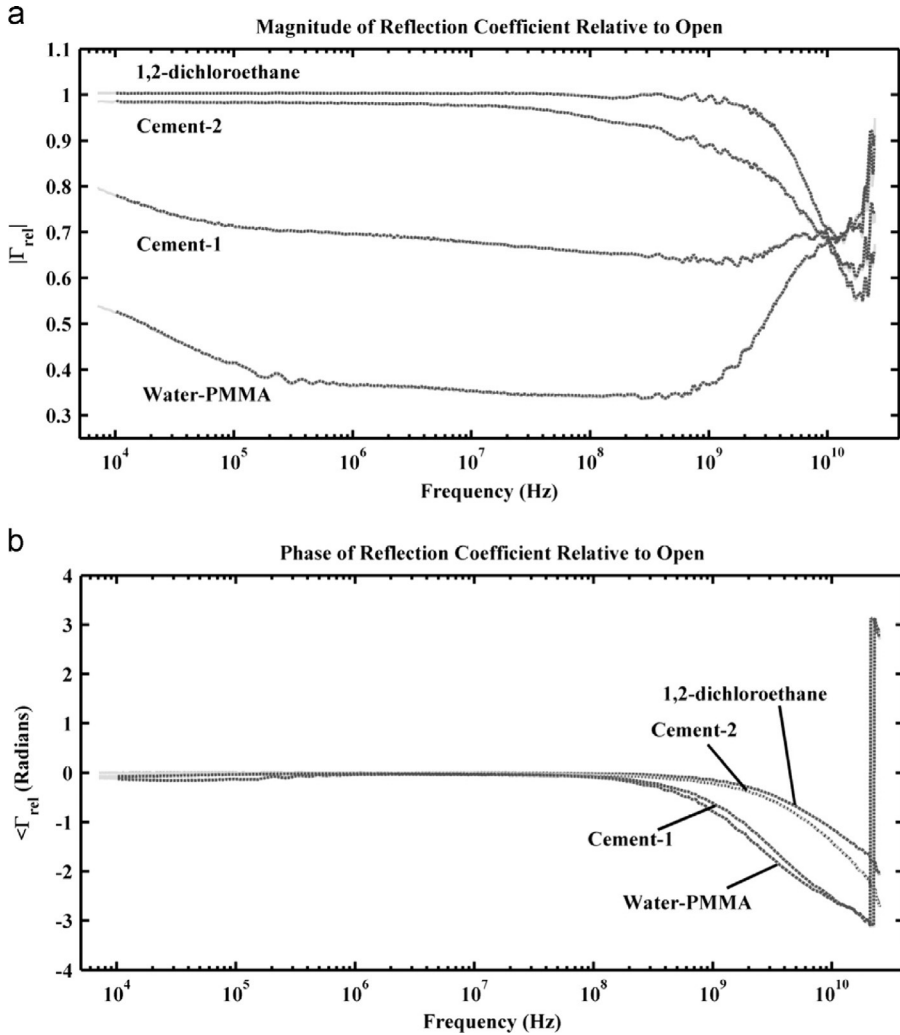


Fig. 6. Comparison of the relative (to open probe) reflection coefficients obtained using the multi-window FFT (solid lines) and the Laplace numerical integration (dashed lines) methods for the four test samples; a) magnitude and b) phase.

These multiple FFT's have to be combined to obtain a single spectrum for the sample. The program stores the truncation frequency points ( $F_{trunc\ i}$ ), which are needed to select a portion of data from each of the FFT windows. The truncation frequency points for each window are assigned based on the sampling frequency to avoid capturing aliased frequencies. Table 1 shows the parameters of the windows used to obtain the FFT for the samples. Sixteen windows used in this paper demonstrate an improvement over twelve windows used in our preliminary study [15].

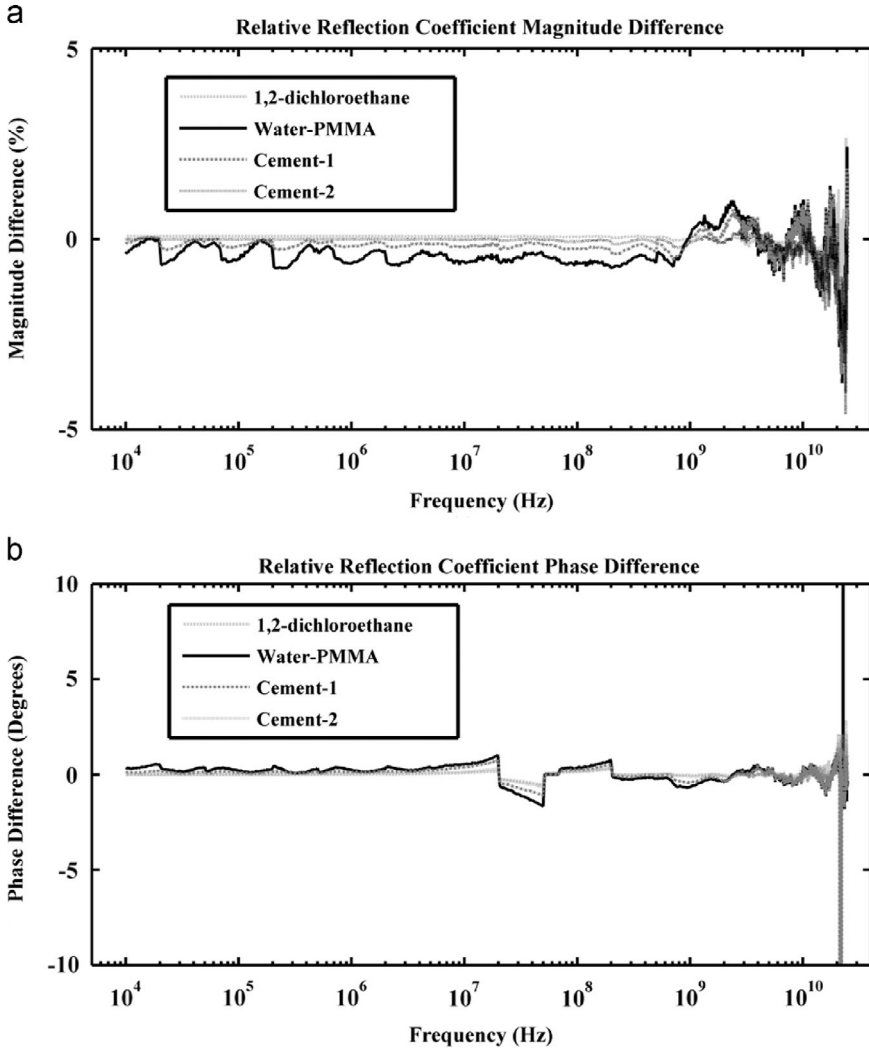


Fig.7. Differences for the relative reflection coefficients' a) magnitude ( $(|\Gamma_{rel}|)_{FFT} - (|\Gamma_{rel}|)_{Laplace} / (|\Gamma_{rel}|)_{Laplace}$ , in percent) and b) phase ( $(\angle\Gamma_{rel})_{FFT} - (\angle\Gamma_{rel})_{Laplace}$ , in degrees) between the multi-window FFT and the numerical Laplace integration.

#### 4. Results

The time domain measurements obtained from TDR are transformed to the frequency domain using our proposed multi-window FFT method with  $N=8192$ . TDR method assumes reflection from open as an approximation of the incident pulse. The open-ended measurement is then used for calculating the relative reflection coefficient,  $\Gamma_{rel}$  [10].  $\Gamma_{rel}$ , relative to the open (empty) sensor, is obtained by dividing the FFT of the sample liquids by the FFT of the empty sensor,  $\Gamma_{rel} = \Gamma_x / \Gamma_r$  [10], where  $\Gamma_x$  and  $\Gamma_r$  are the absolute (true) reflection coefficients for the sample and empty sensor reflections, respectively [10].

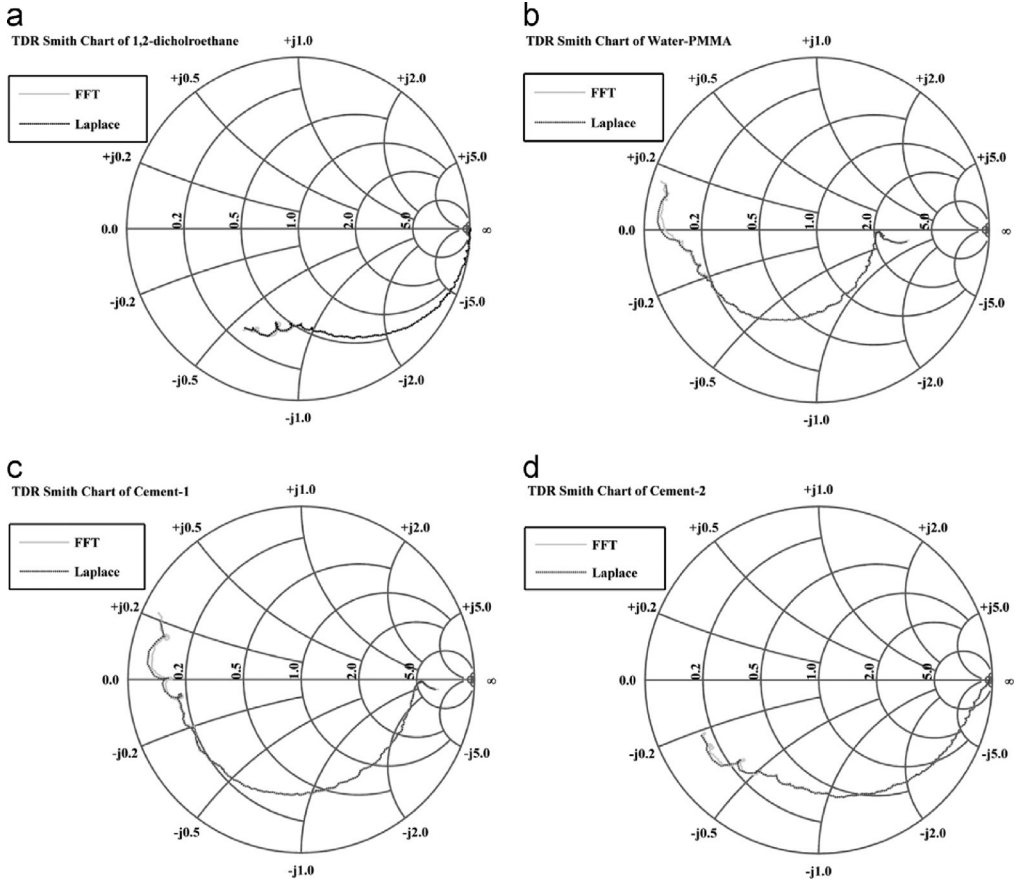


Fig. 8. Smith chart showing the relative (to open) reflection coefficient (polar format) obtained using the multi-window FFT (solid lines) and Laplace numerical integration (dashed lines) methods for the four test samples; a) 1,2 dichloroethane, b) water-PMMA, c) cement-1, and d) cement-2.

Prior to transforming the time domain measurement data to the frequency domain, averaging, smoothing, and interpolation are performed on the raw TDR data (Fig. 5) to reduce noise-like artifacts from the high frequency components of the frequency spectrum. We compare our multi-window FFT method with the existing numerical Laplace integration method [5,6,10] in Fig. 6. This figure demonstrates very close agreement between the two methods. Differences for magnitude (percent) and phase (degrees) between the multi-window FFT and the numerical Laplace integration are illustrated in Fig. 7(a) and (b) respectively. Below 20 GHz, the differences are less than 2% for the magnitude and  $1.7^\circ$  for the phase respectively.

Smith chart plots of  $\Gamma_{rel}$  of the four samples are shown in Fig. 8. Smith chart can serve as a valuable tool for multi-GHz spectra, from which measurement systematic artifacts could be readily identified as discussed in [10].

## 5. Conclusions and future work

This work presents a new methodology to aid broadband material characterization using time domain measurements obtained from TDR. We employ a multi-window method to transform the time domain measurement data to frequency domain using FFT instead of direct

numerical integration of Laplace transform often used in material spectroscopy from TDR data. The results shown in this paper are in excellent agreement with those obtained using the direct numerical integration method.

The method presented in this paper could be used for emerging applications in biology and material science for which dielectric spectroscopy is utilized to understand the state and properties of various materials. Moreover, the FFT algorithm permits efficient and real time implementation of time to frequency conversion of the TDR data utilizing fast hardware platforms such as field-programmable gate arrays (FPGA). For future work, we will use the spectral domain reflection coefficient data obtained by this new method for extracting the complex permittivity of lossy materials to assess its effectiveness in dielectric spectroscopy using the TDR method.

## References

- [1] C.Palego, C.Merla, Y.Ning, C.R.Multari, X.Cheng, D.G.Molinero, G.Ding, X.Luo, J.C.M.Hwang, Broadband microchamber for electrical detection of live and dead biological cells, in: Proceedings of the IEEE International Microwave Symposium, IMS, 2013 (3p.).
- [2] M.R.Tofighi, A.S.Daryoush, Study of the activity of neurological cell solutions using complex permittivity measurement, in: Proceedings of the IEEE International Microwave Symposium, IMS, 2002, pp. 1763–1766.
- [3] K.Grenier, D.Dubuc, P.-E.Poleni, M.Kumemura, H.Toshiyoshi, T. Fujii, H.Fujita, New broadband and contact less RF/microfluidic sensor dedicated to bioengineering, in: Proceedings of the IEEE International Microwave Symposium, IMS, 2009, pp. 1329–1332.
- [4] S.Seo, T.Stintzing, I.Block, D.Pavlidis, M.Rieke, P.G.Layer, High frequency wideband permittivity measurements of biological substances using coplanar waveguides and application to cell suspensions, in: Proceedings of the IEEE International Microwave Symposium, IMS, 2008, pp. 915–918.
- [5] N.E. Hager III, R.C. Domszy, Monitoring of cement hydration by broadband time-domain-reflectometry dielectric spectroscopy, *J. Appl. Phys.* 96 (9) (2004) 5117–5128.
- [6] N.E.Hager III, R.C.Domszy, Time domain reflectometry complex permittivity measurement in hydrating cement systems for determining chemical state of water, in: Proceedings of the 2nd International Symposium on Soil Water Measurement using Capacitance, Impedance, and Time Domain Transmission, 2007, USDA/ARS.
- [7] J. Zhuang, W. Ren, Y. Jing, J.F. Kolb, Dielectric evolution of mammalian cell membranes after exposure to pulsed electric fields, *IEEE Trans. Dielectr. Electr. Insul.* 19 (2) (2012) 609–622.
- [8] H.P.Schwan, Dielectric properties of biological tissue and biophysical mechanisms of electromagnetic-field interaction, in: Proceedings of the ACS Symposium Series, Biological Effects of Nonionizing Radiation, 1981, pp. 109–131.
- [9] T.P. Marsland, S. Evans, Dielectric measurements with an open-ended coaxial probe, *IEE Proc. – Part H: Microw. Antennas Propag.* 134 (4) (1987) 341–349.
- [10] N. Hager, R.C. Domszy, M.R. Tofighi, Smith-chart diagnostics for multi-GHz time-domain-reflectometry dielectric spectroscopy, *Rev. Sci. Instrum.* 83 (2) (2012) 1–11.
- [11] N.E.Hager, R.C.Domszy, M.R.Tofighi, Multi-GHz monitoring of cement hydration using time-domain-reflectometry dielectric spectroscopy, in: Proceedings of the 4th International Symposium on Soil Water Measurement using Capacitance, Impedance and TDT, 2014.
- [12] I.V. Ermolina, E.A. Polygalov, G.D. Romanychev, Y.F. Zuev, Y.D. Feldman, Time domain dielectric spectroscopy with nonuniform signal sampling, *Rev. Sci. Instrum.* 62 (9) (1991) 2262–2265.
- [13] A.M. Nicolson, Forming the fast Fourier transform of a step response in time-domain metrology, *Electron. Lett.* 9 (14) (1973) 317–318.
- [14] A.V. Oppenheim, R.W. Schaffer, *Digital Signal Processing*, Prentice Hall, Eaglewood Cliffs, NJ, 1975.
- [15] A.Bandla, N.E.Hager, M.R.Tofighi, Ultra-broadband material spectroscopy from scattering parameters obtained from time domain measurements,” in: Proceedings of the IEEE Benjamin Franklin Symposium on Microwave and Antenna Sub-Systems for Radar, Telecommunications, BenMAS, 2014, (3 p.).